31st Annual International Conference of the IEEE EMBS
Minneapolis, Minnesota, USA, September 2-6, 2009

Gradient-Driven Beamforming for Biomedical Ultrasound

Solmaz Khezerloo and Daler Rakhmatov

***Abstract*— Adaptive beamforming can significantly improve the image quality in biomedical ultrasound by reducing the clutter due to interfering signals arriving from undesired directions. We consider the conventional linearly constrained minimum variance (LCMV) adaptive beamformer and propose an alternative based on the well-known generalized sidelobe canceller (GSC) whose adaptation relies on unconstrained gradient-driven optimization. The GSC, coupled with iterative optimization methods, allows for a tradeoff between computational complexity of beamforming and the image quality. To the authors' knowledge, this is the first time a GSC-based gradient-driven approach has been applied and evaluated in the context of ultrasound beamforming.**

***Index Terms*— Biomedical signal processing, Array signal processing, Unconstrained optimization methods**

I. Introduction

In biomedical ultrasound imaging systems, a transducer array transmits short pulses and detects returning echos produced by complex tissues and organ boundaries. Received signals are focused using appropriate time delays and then summed, as shown in Figure 1 for a transducer array with M active elements. The weights $w_1, w_2, ..., w_M$ can be based on some fixed apodization window function, or alternatively, they can be computed adaptively based on the properties of received data. Applying the weights, or beamforming, should minimize the contribution of undesired (interfering) signals, thus improving the ultrasound image quality (e.g., resolution and contrast).

The subject of this paper is linearly constrained minimum variance (LCMV) adaptive beamforming, which is one of the earliest and simplest adaptive methods [1]. The LCMV method has recently been applied to biomedical ultrasound, demonstrating significant improvements in image resolution and contrast [2]–[7]. It is possible to produce the same beamforming output using the generalized sidelobe canceller (GSC) structure [1], as shown in Figure 2 and discussed in Section III. The GCS structure arises naturally, when one considers using unconstrained gradient-driven search to find a solution to a constrained optimization problem such as LCMV beamforming. The main advantage of the GSC, coupled with iterative optimization methods, is that its output quality can be traded off for a lower computational cost depending on the number of iterations per input snapshot.

As another alternative to the conventional LCMV method for ultrasound beamforming, we also (briefly) describe and evaluate a simple idea of updating the apodization weights at a reduced rate. In other words, we allow the LCMV beamformer to take more than one sampling period to compute and apply the weights. In the case of the 1/4-rate updating, for example, the beamformer takes as many as four sampling periods (rather than one period) to find the weights and compute the corresponding output (the same weights are applied per four buffered input snapshots). This approach reduces the computational cost per sampling period at the expense of apodization optimality. More details are provided in Section IV.

This work was supported in part by the Natural Sciences and Engineering Research Council of Canada and Canadian Microelectronics Corporation.

The authors are with the Electrical and Computer Engineering Department, University of Victoria, 3800 Finnerty Road, Victoria, British Columbia, V8P 5C2, Canada (Email: daler@uvic.ca).

II. Conventional LCMV Beamformer

Given the beamforming structure in Figure 1, at the sampling instance t, we have the input vector $\mathbf{u}(t) = [u_1(t)\ u_2(t)\ ...\ u_M(t)]^T$. The beamformer output $y(t)$ and output power $P(t)$ are [1]:

$$y(t) = \mathbf{w}(t)^H \mathbf{u}(t), \tag{1}$$

$$P(t) = E[|y(t)|^2] = \mathbf{w}(t)^H \mathbf{R}(t) \mathbf{w}(t), \tag{2}$$

where $\mathbf{w}(t) = [w_1(t)\ w_2(t)\ ...\ w_M(t)]^T$ is the weight vector, and $\mathbf{R}(t) = E[\mathbf{u}(t)\mathbf{u}(t)^H]$ is the spatial covariance matrix. Superscript H indicates conjugate transposition. In our case, all vectors and matrices of interest are real-valued, and H can be replaced with superscript T indicating ordinary transposition.

Let $\mathbf{d}$ denote the steering vector (desired direction) – delay focusing makes it a vector of M ones, i.e., $\mathbf{d} = [1\ 1\ ...\ 1]^T$. The linearly constrained minimum variance (LCMV) beamformer has $\mathbf{w}(t)$ such that signals from the desired direction are passed with a unit gain, while signals from any other direction are suppressed. Equivalently, $\mathbf{w}(t)$ is a solution to the problem of minimizing the LCMV beamformer's output power $P(t)$ subject to the constraint $\mathbf{w}(t)^H \mathbf{d} = 1$. Optimal $\mathbf{w}(t)$ is given by [1]:

$$\mathbf{w}(t) = \frac{\mathbf{R}(t)^{-1}\mathbf{d}}{\mathbf{d}^H \mathbf{R}(t)^{-1}\mathbf{d}}. \tag{3}$$

The spatial covariance matrix $\mathbf{R}(t)$ is usually estimated based on the sample correlation matrix $\widehat{\mathbf{R}}(t)$:

$$\widehat{\mathbf{R}}(t) = \frac{1}{N} \sum_{n=t-N+1}^{t} \mathbf{u}(n)\mathbf{u}(n)^H, \tag{4}$$

where $\mathbf{u}(n)$ is the n-th input snapshot, and N is the number of snapshots. As ultrasound signals are non-stationary, N is usually very small. Coherence between desired signals and interfering signals is another important issue in biomedical ultrasound. The LCMV beamformer performs poorly given

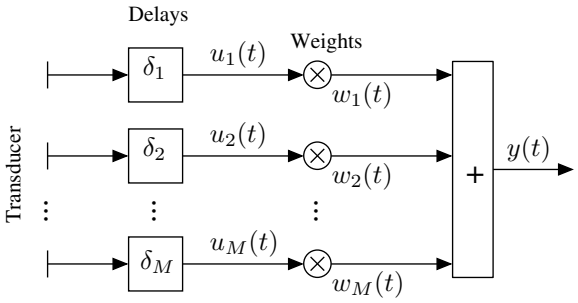

Fig. 1. Conventional ultrasound beamformer.

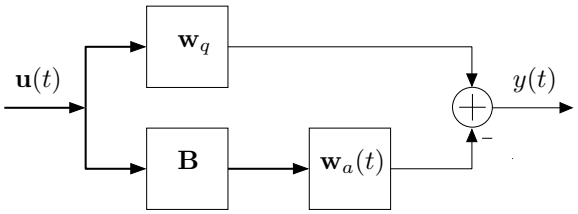

Fig. 2. Generalized sidelobe canceller.

coherent signals, unless we apply certain data preprocessing schemes to create artificial decorrelation [3]. One of such schemes is spatial smoothing [8], which will be used here. Spatial smoothing is based on combining L-element overlapping subarrays of the original M-element array ($L \leq M/2$). Let $\mathbf{x}_k(t) = [u_k(t)\ u_{k+1}(t)\ ...\ u_{k+L-1}(t)]^T$ denote the k-th subarray within $\mathbf{u}(t)$. Then, the spatially smoothed sample correlation matrix $\widetilde{\mathbf{R}}(t)$ is defined as [8]:

$$\widetilde{\mathbf{R}}(t) = \frac{1}{(M-L+1)N} \sum_{n=t-N+1}^{t} \sum_{k=1}^{M-L+1} \mathbf{x}_k(n)\mathbf{x}_k(n)^H. \tag{5}$$

The size of $\widetilde{\mathbf{R}}(t)$ is $L \times L$, whereas the size of $\mathbf{R}(t)$ is $M \times M$. Consequently, using Equation (3) with $\widetilde{\mathbf{R}}(t)$ will produce a weight vector of size L rather than M. We denote this vector by $\widetilde{\mathbf{w}}(t)$:

$$\widetilde{\mathbf{w}}(t) = \frac{\widetilde{\mathbf{R}}(t)^{-1}\mathbf{d}}{\mathbf{d}^H\widetilde{\mathbf{R}}(t)^{-1}\mathbf{d}}. \tag{6}$$

Then, the beamformer output can be computed as follows [3]:

$$y(t) = \frac{1}{M-L+1} \sum_{k=1}^{M-L+1} \widetilde{\mathbf{w}}(t)^H \mathbf{x}_k(t). \tag{7}$$

Figures 3 and 4, obtained with the FIELD II simulation tool [9], illustrate the advantage of the LCMV beamformer (with spatial smoothing) over two non-adaptive beamformers that use either uniform weighting (delay-and-sum) or an apodization function (here, Kaiser window configured for 46-dB sidelobe attenuation). Figure 3 shows that the LCMV beamformer (using a single snapshot: $N = 1$) gives a better resolution. Figure 4 shows that the LCMV beamformer (using two snapshots: $N = 2$) gives a better contrast against speckled background; we found that using two snapshots in this case produces a better-quality image.

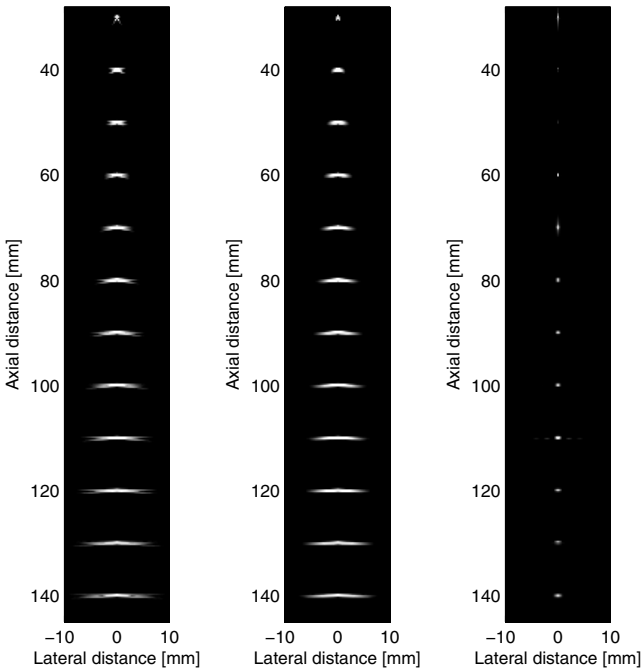

Fig. 3. Performance of delay-and-sum (left), Kaiser window (center), and LCMV (right) beamformers: 12 single point phantoms placed in 10-mm intervals, 64 image lines, 4-MHz 96-element phased array transducer (96 active elements, transmit focus at 60 mm, dynamic receive focus at 10 mm intervals), spatial smoothing with $L = 48$, using one snapshot ($N = 1$).

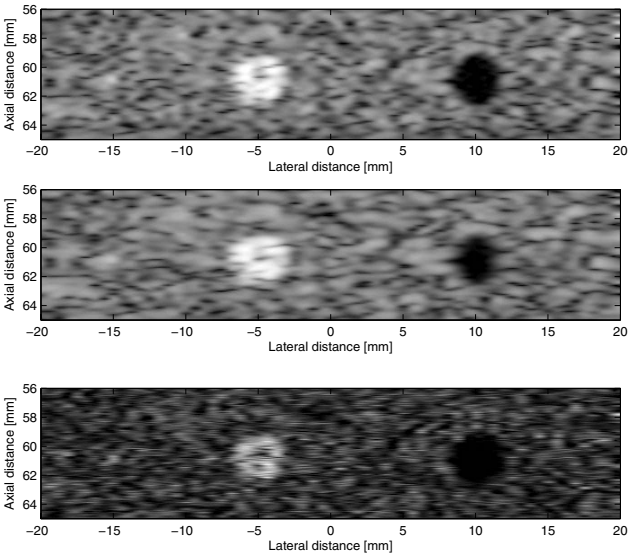

Fig. 4. Performance of delay-and-sum (top), Kaiser window (center), and LCMV (bottom) beamformers: point-scatterer-cyst phantom placed at 60 mm (lateral placement: single point at -15 mm, 3-mm scattering region at -5 mm, 4-mm water-filled cyst at 10 mm), 64 image lines, 3-MHz 192-element linear array transducer (64 active elements, transmit focus at 60 mm, dynamic receive focus at 10 mm intervals), spatial smoothing with $L = 32$, using two snapshots ($N = 2$).

III. Ultrasound Beamforming with GSC

The GSC output is given by [1]:

$$y(t) = [\mathbf{w}_q - \mathbf{B}\mathbf{w}_a(t)]^H \mathbf{u}(t), \quad (8)$$

where $\mathbf{B}$ is the blocking matrix, $\mathbf{w}_q$ and $\mathbf{w}_a(t)$ are the non-adaptive (quiescent) and adaptive weight vectors, respectively. One can interpret $[\mathbf{w}_q - \mathbf{B}\mathbf{w}_a(t)]$ as the weight vector $\mathbf{w}(t)$ of the LCMV beamformer without spatial smoothing. Provided that delay focusing is present (i.e., $\mathbf{d}$ is a vector of M ones), $\mathbf{w}_q$ and $\mathbf{B}$ are fixed, while $\mathbf{w}_a(t)$ varies to enable adaptive response. To match the LCMV beamformer behavior, we want to minimize the output power $P(t)$, while passing the desired signal with a unit gain, and we also want to incorporate spatial smoothing. The unit gain constraint is satisfied by setting $\mathbf{w}_q = (1/M)\mathbf{d}$ and by having $\mathbf{B}$ such that $\mathbf{B}^H\mathbf{d} = \mathbf{0}$ [1].[1] The output power is minimized by updating $\mathbf{w}_a$ based on the gradient $\mathbf{g} = \nabla P$ and the Hessian $\mathbf{H} = \nabla^2 P$ (both with respect to $\mathbf{w}_a$). Without spatial smoothing, we would have

$$\mathbf{g}(t) = -2\mathbf{B}^H\widehat{\mathbf{R}}(t)[\mathbf{w}_q - \mathbf{B}\mathbf{w}_a(t)], \quad (9)$$

$$\mathbf{H}(t) = 2\mathbf{B}^H\widehat{\mathbf{R}}(t)\mathbf{B}. \quad (10)$$

With spatial smoothing, however, we want to use $\widetilde{\mathbf{R}}(t)$ whose size ($L \times L$) is smaller than that of $\widehat{\mathbf{R}}(t)$. Consequently, the sizes of $\mathbf{w}_a$, $\mathbf{w}_q$, and $\mathbf{B}^H$ must be adjusted accordingly. Using symbol $\widetilde{\ }$ to indicate a size reduction due to the presence of spatial smoothing, we now re-define $\mathbf{g}$ and $\mathbf{H}$ as follows:

$$\mathbf{g}(t) = -2\widetilde{\mathbf{B}}^H\widetilde{\mathbf{R}}(t)[\widetilde{\mathbf{w}}_q - \widetilde{\mathbf{B}}\widetilde{\mathbf{w}}_a(t)], \quad (11)$$

$$\mathbf{H}(t) = 2\widetilde{\mathbf{B}}^H\widetilde{\mathbf{R}}(t)\widetilde{\mathbf{B}}. \quad (12)$$

Next, we consider four options for updating $\widetilde{\mathbf{w}}_a(t)$, based on the following four gradient-driven optimization methods [10]. (We take advantage of the fact that the optimization problem at hand is convex quadratic: our objective function P is quadratic, and its Hessian $\mathbf{H}$ is positive definite; hence, no line search is required.)

Newton Method: (13)

$$\widetilde{\mathbf{w}}_{a[i+1]}(t) = \widetilde{\mathbf{w}}_{a[i]}(t) - \mathbf{H}(t)^{-1}\mathbf{g}_{[i]}(t),$$

Quasi-Newton (QN) Method: (14)

$$\widetilde{\mathbf{w}}_{a[i+1]}(t) = \widetilde{\mathbf{w}}_{a[i]}(t) - \frac{\mathbf{g}_{[i]}(t)^T(\mathbf{S}_{[i]}(t)\mathbf{g}_{[i]}(t))}{(\mathbf{S}_{[i]}(t)\mathbf{g}_{[i]}(t))^T\mathbf{H}(t)(\mathbf{S}_{[i]}(t)\mathbf{g}_{[i]}(t))}(\mathbf{S}_{[i]}(t)\mathbf{g}_{[i]}(t)),$$

Steepest Descent (SD) Method: (15)

$$\widetilde{\mathbf{w}}_{a[i+1]}(t) = \widetilde{\mathbf{w}}_{a[i]}(t) - \frac{\mathbf{g}_{[i]}(t)^T\mathbf{g}_{[i]}(t)}{\mathbf{g}_{[i]}(t)^T\mathbf{H}(t)\mathbf{g}_{[i]}(t)}\mathbf{g}_{[i]}(t),$$

Conjugate Gradient (CG) Method: (16)

$$\widetilde{\mathbf{w}}_{a[i+1]}(t) = \widetilde{\mathbf{w}}_{a[i]}(t) + \frac{\mathbf{g}_{[i]}(t)^T\mathbf{g}_{[i]}(t)}{\mathbf{s}_{[i]}(t)^T\mathbf{H}(t)\mathbf{s}_{[i]}(t)}\mathbf{s}_{[i]}(t),$$

[1]For example, given $M = 4$ we have $\mathbf{B} = \begin{bmatrix} 1 & 0 & 0 \\ -1 & 1 & 0 \\ 0 & -1 & 1 \\ 0 & 0 & -1 \end{bmatrix}$.

where i is the iteration number, $\mathbf{S}_{[i]}(t)$ is a special matrix that progressively converges to $\mathbf{H}(t)^{-1}$ as i increases, and $\mathbf{s}_{[i]}(t)$ is a conjugate search direction. We compute $\mathbf{S}_{[i]}(t)$ using the Broyden-Fletcher-Goldfarb-Shanno (BFGS) formula, and we update $\mathbf{s}_{[i]}(t)$ as follows [10]: $\mathbf{s}_{[i+1]}(t) = -\mathbf{g}_{[i+1]}(t) + \frac{\mathbf{g}_{[i+1]}(t)^T\mathbf{g}_{[i+1]}(t)}{\mathbf{g}_{[i]}(t)^T\mathbf{g}_{[i]}(t)}\mathbf{s}_{[i]}(t)$.

Note that we permit multiple iterations per snapshot (i.e., per fixed t).[2] For the current snapshot at time t, we initialize $\widetilde{\mathbf{w}}_a$ to the the vector produced by the last iteration for the previous snapshot: $\widetilde{\mathbf{w}}_{a[0]}(t) = \widetilde{\mathbf{w}}_a(t-1)$. In the special case of a single iteration per snapshot, we obtain the usual form of an adaptive weight update [11]: $\widetilde{\mathbf{w}}_a(t) = \widetilde{\mathbf{w}}_a(t-1) - ....$

Given $\widetilde{\mathbf{B}}$, $\widetilde{\mathbf{w}}_q$, and final $\widetilde{\mathbf{w}}_a(t)$, we can compute the output of the GSC combined with spatial smoothing as follows:

$$y(t) = \frac{1}{M-L+1}\sum_{k=1}^{M-L+1}[\widetilde{\mathbf{w}}_q - \widetilde{\mathbf{B}}\widetilde{\mathbf{w}}_a(t)]^H\mathbf{x}_k(t). \quad (17)$$

One can interpret $[\widetilde{\mathbf{w}}_q - \widetilde{\mathbf{B}}\widetilde{\mathbf{w}}_a(t)]$ as the weight vector $\widetilde{\mathbf{w}}(t)$ of the LCMV beamformer with spatial smoothing.

Table I shows computational costs of the conventional LCMV method and the four described GSC-based gradient-driven methods. (In Table I, symbol I denotes the number of iterations per snapshot.) Table II shows numerical values of computational savings for our test examples: see Figures 3-6, where $M = 96$ and $L = 48$ for the single point phantoms, and $M = 64$ and $L = 32$ for the point-scatterer-cyst phantom. (For the latter, we use $N = 2$, which involves $L(L+1)/2$ extra additions.) These savings are with respect to the baseline cost of the conventional LCMV beamformer. Each entry in Table II is a pair of numbers [Min, Max]. The first number, Min, is computed assuming the same (unit) cost for each addition, multiplication, and square root operation. The second number, Max, is computed assuming that each multiplication is 10 times more expensive than an addition, and each square root operation is 32 times more expensive than an addition. Thus, each reported savings range [Min, Max] captures, to some extent, a variety of possible implementations of adders, multipliers, and square-root circuits. Under such assumptions, the baseline cost of the conventional LCMV beamformer ranges from 54393 to 296226 for the single point phantoms, and from 19297 to 102954 for the point-scatterer-cyst phantom. Note that greater M and L yield greater savings. Next, we take a closer look at the Newton, quasi-Newton, steepest descent, and conjugate gradient methods individually.

A. Newton Method

Replacing $\mathbf{g}_{[i]}(t)$ by $[2\widetilde{\mathbf{B}}^H\widetilde{\mathbf{R}}(t)\widetilde{\mathbf{w}}_q + \mathbf{H}(t)\widetilde{\mathbf{w}}_{a[i]}(t)]$ in Equation (13) yields:

$$\widetilde{\mathbf{w}}_a(t) = 2\mathbf{H}(t)^{-1}\widetilde{\mathbf{B}}^H\widetilde{\mathbf{R}}(t)\widetilde{\mathbf{w}}_q, \quad (18)$$

[2]As ultrasound signals are non-stationary, $\widetilde{\mathbf{R}}(t)$ is usually computed using a very few snapshots, and it may change rapidly with time. Consequently, $\mathbf{H}(t)$ may change rapidly with t as well, per Equation (12). The rationale for permitting multiple iterations per snapshot (i.e., per fixed t) is to facilitate searching with fixed $\mathbf{H}(t)$.

TABLE I

COMPUTATIONAL COST OF BEAMFORMING METHODS UNDER CONSIDERATION.

Method	Additions ($N = 1$)	Multiplications	Square Root
LCMV	$L^3/6 + 2ML - L/6$	$L^3/6 + 3L^2/2 + ML + 13L/3 + 1$	L
Newton	$L^3/6 + 5L^2/2 + 2ML - 14L/3 + 2$	$L^3/6 + 2L^2 + ML - L/6 + 1$	$L - 1$
QN	$2ML + L^2 - 3L + I(7L^2 - 9L - 1)$	$ML + L + 1 + I(8L^2 - 10L + 5)$	0
SD	$2ML + L^2 - 3L + I(2L^2 - 4)$	$ML + L + 1 + I(2L^2 - 1)$	0
CG	$2ML + L^2 - 3L + I(2L^2 + 2L - 6)$	$ML + L + 1 + I(2L^2 + 2L - 2)$	0

that is the Newton method finds optimal $\widetilde{\mathbf{w}}_a(t)$ after a single iteration. The conventional LCMV method also finds the optimal weight vector at once, according to Equation (6). Both methods must compute a product in the form $\mathbf{A}^{-1}\mathbf{b}$, where $\mathbf{A}$ and $\mathbf{b}$ represent either $\widetilde{\mathbf{R}}(t)$ and $\mathbf{d}$ (for conventional LCMV), or $\mathbf{H}(t)$ and $2\widetilde{\mathbf{B}}^H\widetilde{\mathbf{R}}(t)\widetilde{\mathbf{w}}_q$ (for Newton). This product can be computed by solving $(\mathbf{C}\mathbf{C}^H)(\mathbf{A}^{-1}\mathbf{b}) = \mathbf{b}$, where $\mathbf{C}$ is the result of the Cholesky decomposition of $\mathbf{A}$ [12]. Following the standard practice, we first solve $\mathbf{C}\mathbf{a} = \mathbf{b}$ for $\mathbf{a}$, then solve $\mathbf{C}^H(\mathbf{A}^{-1}\mathbf{b}) = \mathbf{a}$ for $(\mathbf{A}^{-1}\mathbf{b})$.

The GSC beamformer based on the Newton method and the conventional LCMV beamformer produce the same-quality output. According to Table II, however, the Newton method does not have a practical advantages over the conventional LCMV beamformer.

TABLE II

NUMERICAL VALUES OF COMPUTATIONAL COSTS IN OUR TEST EXAMPLES (SEE FIGURES 3-6).

Beamforming Method	Savings (%): $M = 96$, $L = 48$	Savings (%): $M = 64$, $L = 32$
Newton	[-11.9, -5.0]	[-14.4, -5.9]
1-iteration QN	[8.7, 14.5]	[-16.0, -8.8]
1-iteration SD	[53.6, 63.3]	[39.2, 52.5]
2-iteration SD	[36.7, 46.2]	[18.0, 30.7]
3-iteration SD	[19.7, 29.1]	[-3.2, 8.8]
4-iteration SD	[2.8, 12.0]	[-24.4, -13.1]
5-iteration SD	[-14.1, -5.1]	[-45.6, -34.9]
1-iteration CG	[53.2, 63.0]	[38.6, 51.9]
2-iteration CG	[36.0, 45.5]	[16.7, 29.3]
3-iteration CG	[18.7, 28.1]	[-5.1, 6.8]
4-iteration CG	[1.4, 10.6]	[-26.9, -15.8]
5-iteration CG	[-15.9, -6.9]	[-48.8, -38.3]

B. Quasi-Newton (QN) Method

Table II shows that, given $M = 96$ and $L = 48$ (the single point phantoms), the QN method with one iteration per snapshot saves approximately 10% of computations. We cannot afford more than one iteration per snapshot, as it would make the QN method more expensive than the conventional LCMV method. The 1-iteration QN method produces poor $\widetilde{\mathbf{w}}_a(t)$, as illustrated by the image quality in Figure 5. The situation is worsened by the fact that $\mathbf{H}(t)$ is time-dependent, which may affect the continuing convergence from the previously computed $\mathbf{S}(t-1)$ to the current $\mathbf{H}^{-1}(t)$. The 1-iteration QN method may offer some practical value when $M = 128$ and $L = 64$ (over 25% savings), but its use still remains weakly motivated due to the poor quality of images. Note that for the point-scatterer-cyst phantom ($M = 64$ and $L = 32$), the conventional LCMV method (producing optimal weights) is less expensive.

C. Steepest Descent (SD) Method

The SD method can afford as many as four iterations per snapshot for the single point phantoms, and three iterations per snapshot for the point-scatterer-cyst phantom, without exceeding the computational cost of the conventional LCMV beamformer. The savings range approximately from 0% to 60%, but we also face a degradation in the image quality, especially in the case of the single point phantoms (see Figure 5). From the practical point of view, the CG method is preferable over the SD method, as the former exhibits faster convergence and has a similar computational cost in comparison to the latter (see Table II).

Remark: The steepest descent method with one iteration per snapshot is closely related to the classical least-mean-squares (LMS) algorithm. Combining spatial smoothing with the GSC based on the LMS algorithm was studied in [13]. Without spatial smoothing, the LMS algorithm would update $\mathbf{w}_a$ as follows [11]:

$$\mathbf{w}_a(t+1) = \mathbf{w}_a(t) + \mu\mathbf{B}^H\mathbf{u}(t)\mathbf{u}(t)^H[\mathbf{w}_q - \mathbf{B}\mathbf{w}_a(t)], \quad (19)$$

where μ is the constant step-size parameter. With spatial smoothing, one can use the following update method from [13]:

$$\begin{aligned}\widetilde{\mathbf{w}}_a(t+1) &= \widetilde{\mathbf{w}}_a(t) + \mu\widetilde{\mathbf{B}}^H\widetilde{\mathbf{R}}(t)[\widetilde{\mathbf{w}}_q - \widetilde{\mathbf{B}}\widetilde{\mathbf{w}}_a(t)] \quad (20)\\ &= \widetilde{\mathbf{w}}_a(t) - \mu\mathbf{g}(t)/2.\end{aligned}$$

The main difference between Equations (20) and (15) is the step-size parameter: in our case, $\mu(t) = \frac{\mathbf{g}(t)^T\mathbf{g}(t)}{\mathbf{g}(t)^T\mathbf{H}(t)\mathbf{g}(t)}$, i.e., it is exactly prescribed, optimal (fastest convergence), and time-dependent.

D. Conjugate Gradient (CG) Method

For the current snapshot at time t, we initialize $\mathbf{s}$ as follows [10]: $\mathbf{s}_{[0]}(t) = -\mathbf{g}_{[0]}(t) = 2\widetilde{\mathbf{B}}^H\widetilde{\mathbf{R}}(t)\widetilde{\mathbf{w}}_q - \mathbf{H}(t)\widetilde{\mathbf{w}}_{a[0]}(t)$. The first iteration of the CG method produces the same results as the first iteration of the SD method, as Equations (15) and (16) become identical for $i = 0$. The subsequent iterations of the CG method are producing better results than those of the SD method, as illustrated by Figures 5 and 6. According to Table II, the computational savings of both methods are comparable to each other, which makes the CG method a preferred choice. Section V provides further details and recommendations based on the evaluation results for our test examples.

TABLE III

NUMERICAL VALUES OF COMPUTATIONAL COSTS IN OUR TEST EXAMPLES (SEE FIGURES 8 AND 10).

Update Rate	Savings (%): $M = 96$, $L = 48$	Savings (%): $M = 64$, $L = 32$
4	[71.7, 74.3]	[66.8, 69.9]
8	[83.6, 86.7]	[80.6, 84.3]
16	[89.6, 92.9]	[87.5, 91.5]

IV. LCMV BEAMFORMING WITH REDUCED-RATE WEIGHT UPDATE

In the previous section we have shown that iterative gradient-driven beamforming, based on the GSC structure, can offer lower computational complexity than that of the conventional LCMV method, but at the expense of the reduced output quality (i.e., the weights are no longer optimal). A similar tradeoff between the computational cost and the output quality can be achieved with a different approach: we are to use the conventional LCMV beamformer, but to reduce the rate at which its weights are computed and applied.

For each sampled input $\mathbf{u}(t)$, the conventional LCMV beamformer finds and applies optimal weights $\widetilde{\mathbf{w}}(t)$ to compute output $y(t)$, according to Equations (6) and (7). Let COST_w and COST_y denote the respective cost of computing the weights and the output for given $\mathbf{u}(t)$. The total cost per sampling period is $(\text{COST}_w + \text{COST}_y)$ for the conventional LCMV beamformer. If we update the weights once every N_w sampling periods (rather than every period), then the cost per sampling period becomes $(\text{COST}_w/N_w + \text{COST}_y)$. Since the total cost is dominated by the cost of computing the weights, the potential savings can be substantial.

Effectively, we want to let the LCMV beamformer take as many as $(N_w - 1)$ extra sampling periods to compute the optimal weights. For a given sampling instance t, the weights are computed based on $\widetilde{\mathbf{R}}(t)$, but they will not be ready for the next $(N_w - 1)$ sampling periods. While waiting for the new weight vector, the beamformer buffers new inputs $\mathbf{u}(t), \mathbf{u}(t+1), ..., \mathbf{u}(t+N_w-1)$ and produces the outputs by applying the previous weight vector, computed based on $\widetilde{\mathbf{R}}(t - N_w)$, to the previously buffered inputs $\mathbf{u}(t-N_w), \mathbf{u}(t-N_w+1), ..., \mathbf{u}(t-1)$. Figures 8 and 10 show that the image quality remains more or less acceptable, when we let $N_w = 4, 8, 16$. Table III shows the corresponding computational savings that range approximately from 70% to 90%.

V. EVALUATION RESULTS

Figures 5 and 6, obtained with the FIELD II simulation tool [9], illustrate the performance of the GSC beamformer based on the QN, SD, and CG methods. The Newton method produces the same output as that of the conventional LCMV method, shown in Figures 3 and 4.

A more detailed picture in the case of single point phantoms is conveyed by Figure 7 that shows the point spread function at the transmit focus. As expected, the conventional LCMV and Newton methods produce identical FWHM (full width at half maximum), mainlobe energy E_{ML}, and sidelobe energy E_{SL} (assuming a 25-dB attenuation threshold): they are the best among all the methods considered here. The performance of the 1-iteration QN method is worse than that of the 3-iteration SD method, and the latter is outperformed by the 3-iteration CG method. Table IV shows the corresponding numerical values of interest. The practical utility of the 1-iteration SD/CG method is limited due to the poor image quality. On the other hand, using 5 iterations for the SD or CG methods exceeds the computational cost of the conventional LCMV beamformer. To strike a reasonable tradeoff, the 3-iteration CG method is recommended, offering approximately 20% in computational savings (see Table II).

TABLE IV

FWHM, SIDELOBE ENERGY E_{SL}, AND MAINLOBE ENERGY E_{ML} AT TRANSMIT FOCUS (SINGLE POINT PHANTOMS).

Beamforming Method	FWHM (mm)	E_{SL} (dB)	E_{ML} (dB)	E_{SL}/E_{ML} (dB)
Delay-and-Sum	0.885	-23.777	2.964	-26.741
Kaiser Window	1.186	-24.770	4.134	-28.903
LCMV/Newton	0.351	-36.919	-1.291	-35.628
1-iteration QN	0.358	-20.962	-1.184	-19.779
1-iteration SD/CG	0.360	-24.259	-1.172	-23.088
3-iteration SD	0.354	-26.410	-1.248	-25.161
5-iteration SD	0.352	-27.138	-1.282	-25.857
3-iteration CG	0.351	-31.910	-1.290	-30.620
5-iteration CG	0.351	-34.030	-1.290	-32.740

Table V shows the contrast values in the case of the point-scatterer-cyst phantom. The object's contrast against background is defined as the ratio $(S_{\text{background}} - S_{\text{object}})/S_{\text{background}}$, where S denotes the average log-compressed signal envelope inside the region of interest. The conventional LCMV and Newton methods produce the best contrast values, as expected. The 1-iteration QN method is not used, as it is more expensive yet suboptimal in comparison to the conventional LCMV beamformer. The 1-iteration SD/CG methods perform relatively well, while using 3 iterations does not produce a considerably better image to justify a considerable reduction in computational savings. Hence, the 1-iteration SD method is recommended, offering approximately 40% in computational savings (see Table II).

Figures 8 and 10 show the simulation results for the single point phantoms and the point-scatterer-cyst phantom, given $N_w = 4, 8, 16$; the point spread function at the transmit focus in the case of single point phantoms is shown Figure 9. Tables VI and VII show the numerical values of interest. The update rate of 1/8 ($N_w = 8$) appears to be a good choice, striking a favorable tradeoff between the image quality and the computational savings (over 80%) in comparison to the cases with $N_w = 4$ and $N_w = 16$ (see Table III).

VI. CONCLUSION

We have described the application of the GSC structure to adaptive ultrasound beamforming as an alternative to the conventional LCMV method. We have considered adjusting the GSC's adaptive weight vector using four gradient-driven methods: Newton, quasi-Newton, steepest descent,

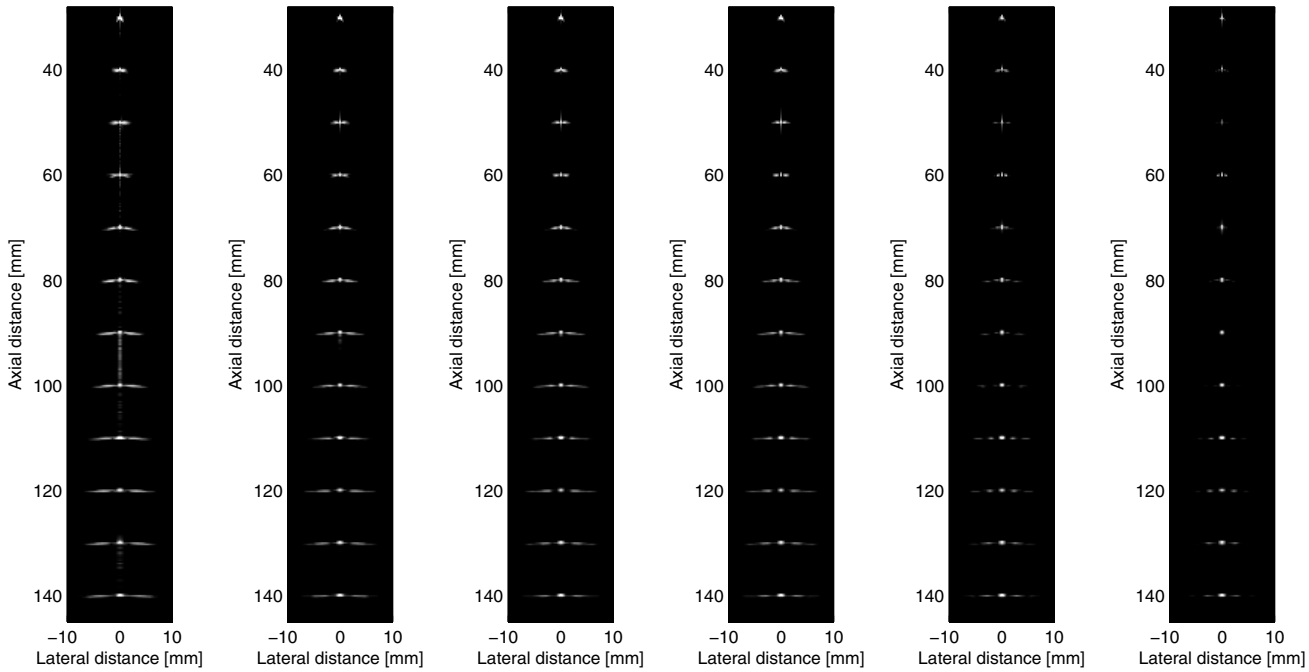

Fig. 5. From left to right: Performance of 1-iteration QN, 1-iteration SD/CG, 3-iteration SD, 5-iteration SD, 3-iteration CG, and 5-iteration CG methods: single point phantoms (cf. Figure 3).

TABLE V

CONTRAST WITH RESPECT TO SPECKLED BACKGROUND (POINT-SCATTERER-CYST PHANTOM).

Beamforming Method	Scattering Region	Water-Filled Cyst
Delay-and-Sum	1.290	0.931
Kaiser Window	1.210	0.888
LCMV/Newton	2.214	0.943
1-iteration SD/CG	1.494	0.931
3-iteration SD	1.696	0.936
3-iteration CG	1.820	0.931

TABLE VI

LCMV WITH REDUCED-RATE UPDATE: FWHM, E_{SL}, E_{ML} AT TRANSMIT FOCUS (SINGLE POINT PHANTOMS).

Update Rate	FWHM (mm)	E_{SL} (dB)	E_{ML} (dB)	E_{SL}/E_{ML} (dB)
1	0.351	-36.919	-1.291	-35.628
1/4	0.360	-26.958	-1.109	-25.894
1/8	0.361	-24.053	-1.120	-22.933
1/16	0.471	-24.560	-1.009	-25.604

TABLE VII

LCMV WITH REDUCED-RATE UPDATE: CONTRAST (POINT-SCATTERER-CYST PHANTOM).

Update Rate	Scattering Region	Water-Filled Cyst
1	2.214	0.943
1/4	2.711	0.968
1/8	1.756	0.918
1/16	1.592	0.886

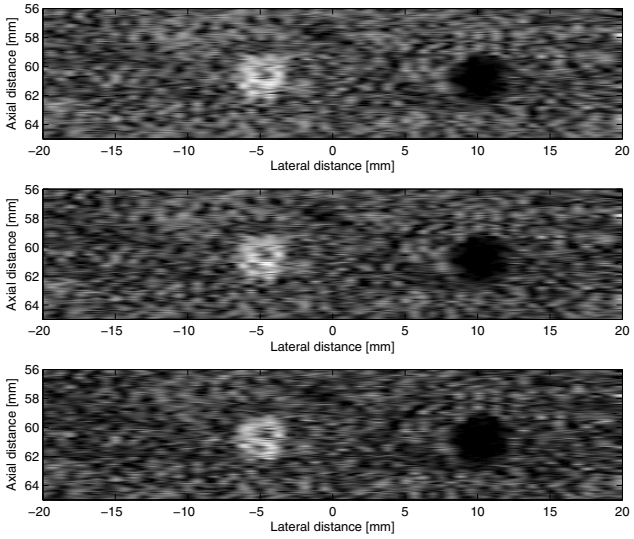

Fig. 6. From top to bottom: Performance of 1-iteration SD/CG (top), 3-iteration SD (center), and 3-iteration CG (bottom) methods: point-scatterer-cyst phantom (cf. Figure 4).

and conjugate gradient. Based on our evaluation results for the single point phantoms, we recommend using the 3-iteration conjugate gradient method, whose computational is approximately 20% less than that of the conventional LCMV beamformer. For the case of the point-scatterer-cyst phantom, we recommend the 1-iteration steepest descent method offering approximately 40% in computational savings. These savings, however, lead to (tolerable) degradation of the image quality. As an alternative approach to lower computational costs, we have also proposed to use the LCMV beamformer whose weights are updated at a reduced rate. A detailed

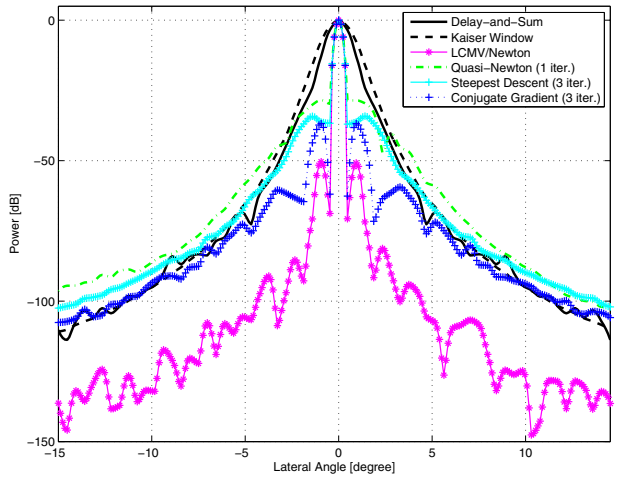

Fig. 7. Point spread function at transmit focus (single point phantoms).

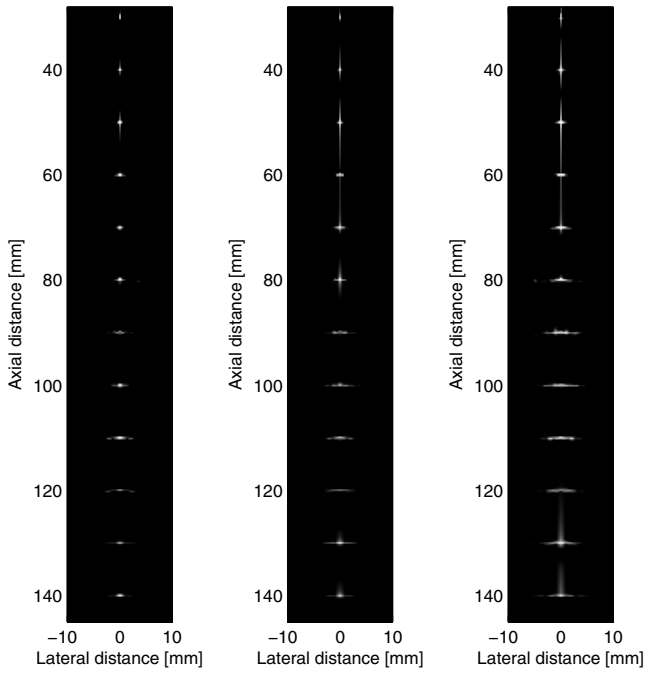

Fig. 8. Performance of LCMV beamformer with 1/4-rate (left), 1/8-rate (center), and 1/16-rate (right) weight updating: single point phantoms (cf. Figure 3).

qualitative and quantitative study of this method is the subject of our future work.

REFERENCES

[1] D. Johnson and D. Dudgeon, *Array Signal Processing*. NJ: Prentice-Hall, 1993.

[2] J. Mann and W. Walker, "A constrained adaptive beamformer for medical ultrasound: Initial results," in *Proc. IEEE Ultrasonics Symp.*, Oct. 2002, pp. 1807–1810.

[3] M. Sasso and C. Cohen-Bacrie, "Medical ultrasound imaging using the fully adaptive beamformer," in *Proc. IEEE International Conf. Acoustics, Speech, and Signal Processing, Vol. II*, Mar. 2005, pp. 489–492.

[4] Z. Wang, J. Li, and R. Wu, "Time-delay- and time-reversal-based robust Capon beamformers for ultrasound imaging," *IEEE Trans. Medical Imaging*, vol. 24, no. 10, pp. 1308–1322, Oct. 2005.

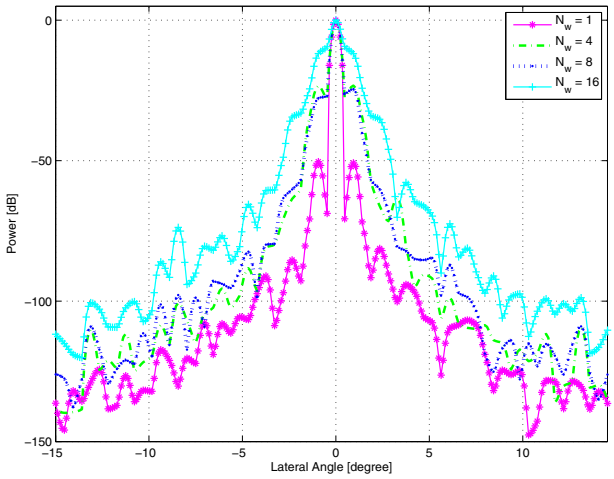

Fig. 9. LCMV with reduced-rate update: Point spread function at transmit focus (single point phantoms).

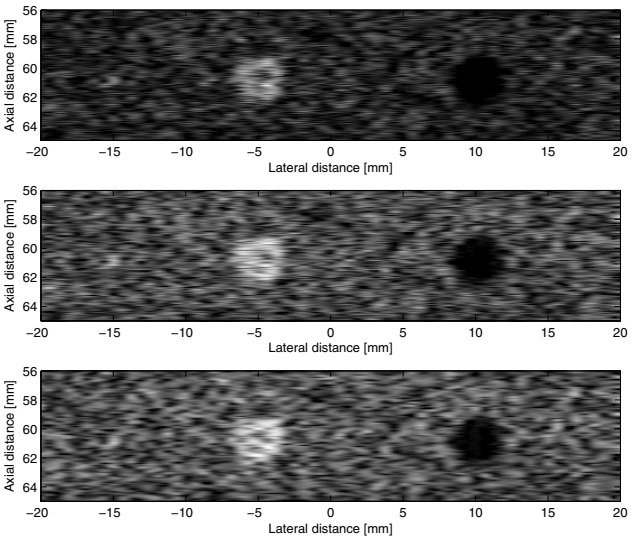

Fig. 10. Performance of LCMV beamformer with 1/4-rate (top), 1/8-rate (center), and 1/16-rate (bottom) weight updating: point-scatterer-cyst phantom (cf. Figure 4).

[5] J. Synnevag, A. Austeng, and S. Holm, "Adaptive beamforming applied to medical ultrasound imaging," *IEEE Trans. Ultrasonics, Ferroelectrics, and Frequency Control*, vol. 54, no. 8, pp. 1606–1613, Aug. 2007.

[6] I. Holfort, F. Gran, and J. Jensen, "Minimum variance beamforming for high frame-rate ultrasound imaging," in *Proc. IEEE Ultrasonics Symp.*, Oct. 2007, pp. 1541–1544.

[7] ——, "Plane wave medical ultrasound imaging using adaptive beamforming," in *Proc. IEEE Sensor Array and Multichannel Signal Processing Workshop*, July 2008, pp. 288–292.

[8] T. Shah and T. Kailath, "Adaptive beamforming for coherent signals and interference," *IEEE Trans. Acoustics, Speech, and Signal Processing*, vol. 33, no. 3, pp. 527–536, June 1985.

[9] J. Jensen, "Field II Simulation Program," 2008, http://server.elektro.dtu.dk/personal/jaj/field.

[10] A. Antoniou and W. Lu, *Practical Optimization*. NY: Springer, 2007.

[11] S. Haykin, *Adaptive Filter Theory*, 4th ed. NJ: Prentice-Hall, 2001.

[12] G. Golub and C. Van Loan, *Matrix Computations*, 3rd ed. MD: Johns Hopkins, 1996.

[13] P. Anderson and M. Ingram, "The performance of the least mean squares algorithm combined with spatial smoothing," *IEEE Trans. Signal Processing*, vol. 45, no. 4, pp. 1005–1012, Apr. 1997.